Classical Hartmann test with scanning

**Rufino Díaz-Uribe[1,*], Fermín Granados-Agustín[2],
and Alejandro Cornejo-Rodríguez[2]**

[1] Universidad Nacional Autónoma de México, Centro de Ciencias Aplicadas y Desarrollo Tecnológico, Apdo. Postal 70-186, C.P. 04510, México, D.F., MÉXICO.
[2] Instituto Nacional de Astrofísica, Óptica y Electrónica, Apdo. Postal 216, C.P. 72000, Puebla, Pue., MÉXICO.
* rufino.diaz@ccadet.unam.mx

Abstract: In order to introduce many more evaluation points during the Hartmann test, the scanning of the screen across the pupil is proposed; after each step of the scan a different image of the bright spots is obtained. Basic ideas about how to design radial and square screens for the scanning are presented. Radial screens are scanned by rotation, whereas for square screens a linear inclined scan is enough to introduce many more evaluation points along two independent directions. For square screens it is experimentally shown that the lateral resolution of the test is improved.

OCIS codes: (220.4840) Testing; (120.3940) Metrology; (120.4800) Optical standards and testing; (120.6650) Surface measurements, figure.

References and links

1. D. Malacara-Doblado, and E. Ghozeil, "Hartmann, Hartmann-Shack and other screen tests," in Optical Shop Testing, Third Edition, Edited by Daniel Malacara (John Wiley and Sons, 2007), Chapter10.
2. A. Morales, and D. Malacara, "Geometrical parameters in the Hartmann test of aspherical mirrors," Appl. Opt. **22**(24), 3957–3959 (1983).
3. V. I. Moreno-Oliva, M. Campos-García, R. Bolado-Gómez, and R. Díaz-Uribe, "Point shifting in the optical testing of fast aspheric concave surfaces by a cylindrical screen," Appl. Opt. **47**(5), 644–651 (2008).
4. D. Liu, H. Huang, B. Ren, A. Zeng, Y. Yan, and X. Wang, "Scanning Hartmann test method and its application to lens aberration measurement," Chin. Opt. Lett. **4**, 725–728 (2006).
5. R. Díaz-Uribe, "Medium-precision null-screen testing of off-axis parabolic mirrors for segmented primary telescope optics: the large millimeter telescope," Appl. Opt. **39**(16), 2790–2804 (2000).
6. M. Avendaño-Alejo, V. I. Moreno-Oliva, M. Campos-García, and R. Díaz-Uribe, "Quantitative evaluation of an off-axis parabolic mirror by using a tilted null screen," Appl. Opt. **48**(5), 1008–1015 (2009).

1. Introduction

The classical Hartmann [1] test makes use of an opaque screen with holes for selecting thin pencils of rays which are used for measuring the transverse aberration of rays reflected on different regions of the surface under test; then, after a numerical integration algorithm (or equivalent procedure), the wavefront aberrations and (or) the shape of the surface and its departures from the ideal surface are calculated. Usually, the number of holes on the Hartmann screen is limited to nearly one hundred [2]; for large astronomical telescope mirrors this number can be increased to several hundred [1]. There are at least two reasons that make it important to have more points to be evaluated on the test surface: first of all, when the trapezoidal rule is used for integrating the transverse aberration, the truncation error increases with the square of the point separation; having more points will reduce the average separation and, in consequence, the truncation error [3]. A second reason is that closer points give more information about higher order aberrations or, equivalently, about higher spatial frequencies of the surface. An important limitation to increasing the number of holes, is the fact that the diameter of the holes cannot be reduced indefinitely, because diffraction effects become important for small hole apertures [2]. In addition, even from a geometrical optics point of view, the light spots at the detector can be so large that they almost overlap each other, so that they cannot be brought closer. A way to increase the number of evaluation points without increasing the number of holes in the Hartmann screen, is to scan the screen across the pupil of the test component; for each position of the screen a different image of the bright spots at

the viewing plane is obtained. During the scan only the screen is moved, so the positions of all the spots of the images can be put together because they give information about the aberration of the same surface; the key point in this method is to have a complete information of the hole positions for each step. As long as the motion of the screen is a rigid body motion, accurate positions of each hole for each step can be obtained from an accurate measurement of the initial positions of the holes (screen calibration) and an accurate measurement of the movements of the screen.

An early proposal for scanning a Hartmann screen was made recently [4]. There, the authors made use of a screen with a certain number of radial lines of holes and rotated the screen to scan the full aperture of the test lens; they discussed the simple case of two lines, with different radial hole positions on each line, however they did not say how many different pairs of lines were used for their experiment.

In this paper we describe some ideas on how to design spiral Hartmann screens in such a way that only by rotating the screen the number of points being evaluated on the surface under test can be multiplied by the number of steps of the scan. In addition, we describe a method for scanning a classical square Hartmann screen by linear translations along its own plane to include new evaluation points in those zones where the evaluation with only one screen position and image, is not possible; there, the surface is only interpolated. This allows an increase of the total number of evaluation points to some hundred or even to more than one thousand points, more or less evenly distributed, by capturing a different image on each step.

2. Spiral screen

Two important conditions must be imposed over the total set of points obtained with a scanning screen: first of all, the obtained points should be more or less evenly distributed in such a way that there must always be a nearby point to follow smooth integration paths avoiding large steps. Secondly, the points must be as orderly as possible; there is no basic restriction on the spatial order of the points, but it is easier to define smooth integration paths with an orderly set than with a randomly positioned set of points.

The spiral screen is designed as follows. Given an initial number of radial lines n and the number of holes m along each line (see Fig. 1.a), the full angle that the screen must be rotated for the scan is

$$\theta = \frac{2\pi}{n}; \qquad (1)$$

the initial radial separation between adjacent holes is

$$a = \frac{D}{2m} \qquad (2)$$

where D is the diameter of the exit pupil of the system under test. Then, giving k, the desired number of new evaluation points (between two originally adjacent holes) to be obtained during the scan, a new set of holes are displaced the distance

$$\Delta a = \frac{a}{k+1} = \frac{D}{2m(k+1)}, \qquad (3)$$

along the radial direction and azimuthally through the angle (see Fig. 1.b)

$$\alpha = \frac{\theta}{k+1}. \qquad (4)$$

The total number of holes on the screen is (see Fig. 1.c)
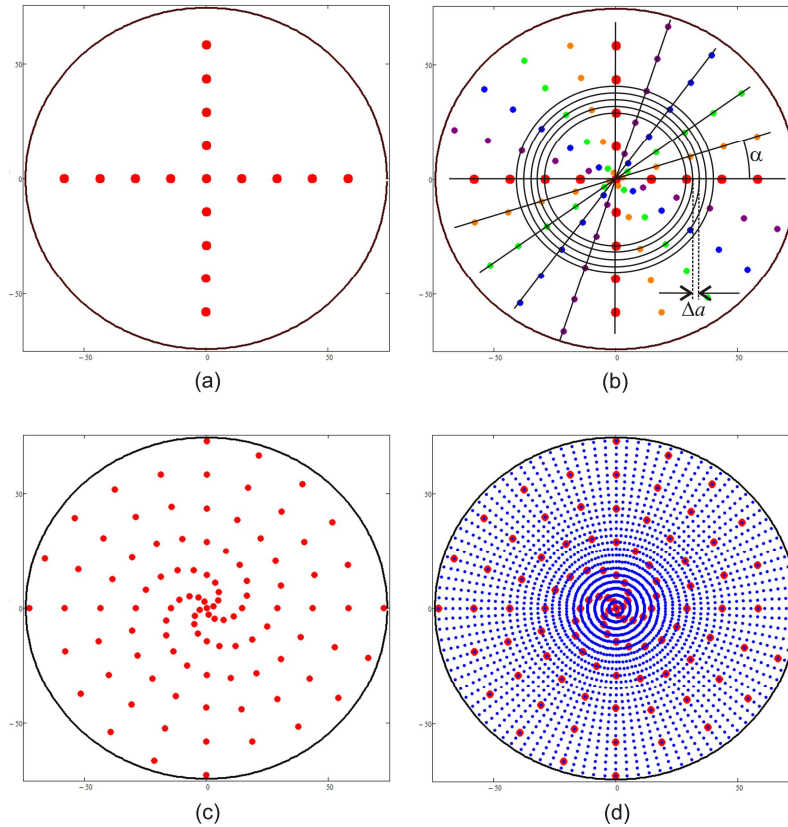
$$N = nm(k+1). \qquad (5)$$

Fig. 1. Design of the spiral screen. a) The basic set of points is defined; in this case $n = 4$, $m = 5$, $\theta = 90°$. b) Additional points are included $k = 5$. c) Final positions for the holes on the screen. d) Rotation of the screen in steps of $\Delta\alpha = 3.6°$ allows testing of the surface at T = 3000 points.

The screen is rotated in

$$s = (k+1)^2 \tag{6}$$

steps of angular size

$$\Delta\alpha = \frac{\alpha}{k+1}. \tag{7}$$

In each step an image of the bright spots at the observing plane is recorded, so the total number of evaluated points is (see Fig. 1.d)

$$T = N(k+1)^2 = nm(k+1)^3 \tag{8}$$

2.1 Hole size

According to A. Morales and D. Malacara [3], in order to have smaller bright spots at the observation plane, the holes in the Hartmann screen must be as small as possible; diffraction effects, however, cause a spreading of the light on the same plane. The optimum size of the holes is given by

$$d_h = \left[\frac{1.63\lambda}{-Kc^3D^2 + 1.33c^2L} \right] \tag{9}$$

where λ is the wavelength of the light used during the test, K is the conic constant of the mirror under test, c is its curvature at the vertex, D its diameter, and L is the distance from the observation plane to the plane where the reflected rays are focused. For a spherical mirror $K = 0$, tested under visible light $\lambda = 500$ nm, $r = 1/c = 600$ mm, $D = 150$mm, the optimum hole size is a function of L; in Fig. 2, a plot of the hole diameter vs. L is shown. It is easy to see that for values of L between 2 and 10 mm, the hole size varies between 10 and 5 mm.
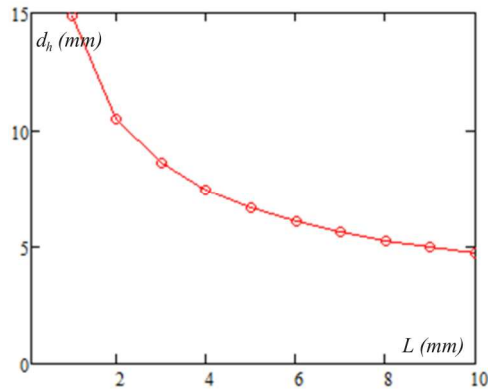

Fig. 2. Optimum hole diameter d_h as a function of the distance L, for $K = 0$, $\lambda = 500$ nm, $r = 1/c$ = 600 mm, $D = 150$mm, according to ref [3] (see Eq. (1).

2.2 Alternative screen designs

Choosing 5 mm as the hole diameter, the spiral screen designed above with $n = 4$, $m = 5$, and $\theta = 90°$, is as shown in Fig. 3. It is clear that for spiral screens, the azimuthal distance between adjacent holes depends on the distance to the center of the screen; adding size to the holes, at the center of the screen, they overlap whereas at the rim they are more separated. Then, with this kind of screen the wavefront is not uniformly sampled; scanning the screen increases the number of points but the sampling is still not uniform.
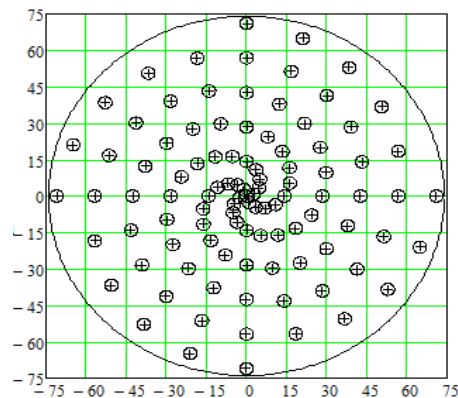

Fig. 3. Spiral screen as designed in Fig. 1 (c), with finite hole size. The superposition at the center is evident. Units are mm.

Alternative designs can be obtained increasing the numbers n and m, and locating a hole only on these points where the overlap is not present; the other points are not included. For instance, in Fig. 4 a different screen design is obtained for $n = m = 20$; the small dots are the points obtained with the first proposal above, whereas the circles with the plus signs in the center describe the holes and their centers with a more uniform distribution without overlapping. In Fig. 5, some simulations of scanning the screen in Fig. 4 are shown for the cases with $t = 4, 8, 12, 17$, and 32; each angular step is given by $\gamma = 2\pi / t$. Evidently, many

new evaluation points are added but at the center and its neighborhood there are large zones without evaluation points.
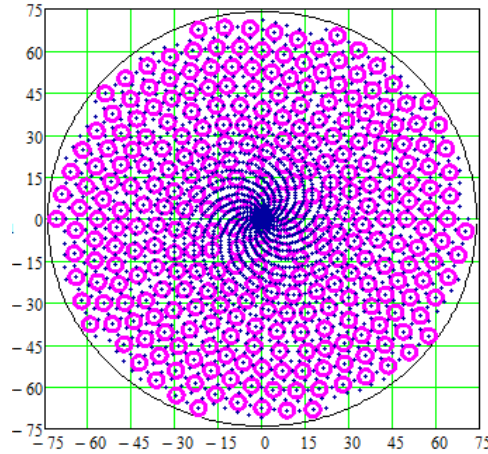

Fig. 4. Spiral screen without overlapping; a more uniform sampling is made.

A last attempt to use the modified spiral screens but trying to cover these empty zones, is to rotate the screen around a point different from the center. Figure 6 shows an example of this, of course at the center of the screen the empty areas are smaller, but the whole set of points become a more random spatial distribution, making difficult to define integration paths in an easy way.

Perhaps an additional study of these ideas can give an appropriate screen design and scan method, however we found that a square screen is more convenient for the improvement of the Hartmann test, as is shown in the next section.

3. Square screen

In the search to overcome the drawbacks of the spiral screens described previously, it was found that a classical square Hartmann screen can be used for the scanning test. At the early stages of this study, it seemed to be necessary to scan the screen along two different directions, however, a little thinking on the problem shown that it is sufficient to move the screen along a single direction, different from the principal directions of the hole array. For this, the screen must be larger than the diameter of the test surface. If the separation of center points of the holes on the screen is defined by

$$c = \frac{D}{m-1},\tag{10}$$

where m is the number of points along one principal diameter of the mirror under test, the number of points inside the pupil is approximately given by

$$N \approx \frac{\pi(m-1)^2}{4}.\tag{11}$$

The scan length and direction can be selected at will; in order to explain the proposal in a more systematic way, however, let us choose the scan direction along the line defined by two holes P1 and P2, in different but adjacent rows and in different columns separated a distance (see Fig. 7)

$$d' = cb,\tag{12}$$
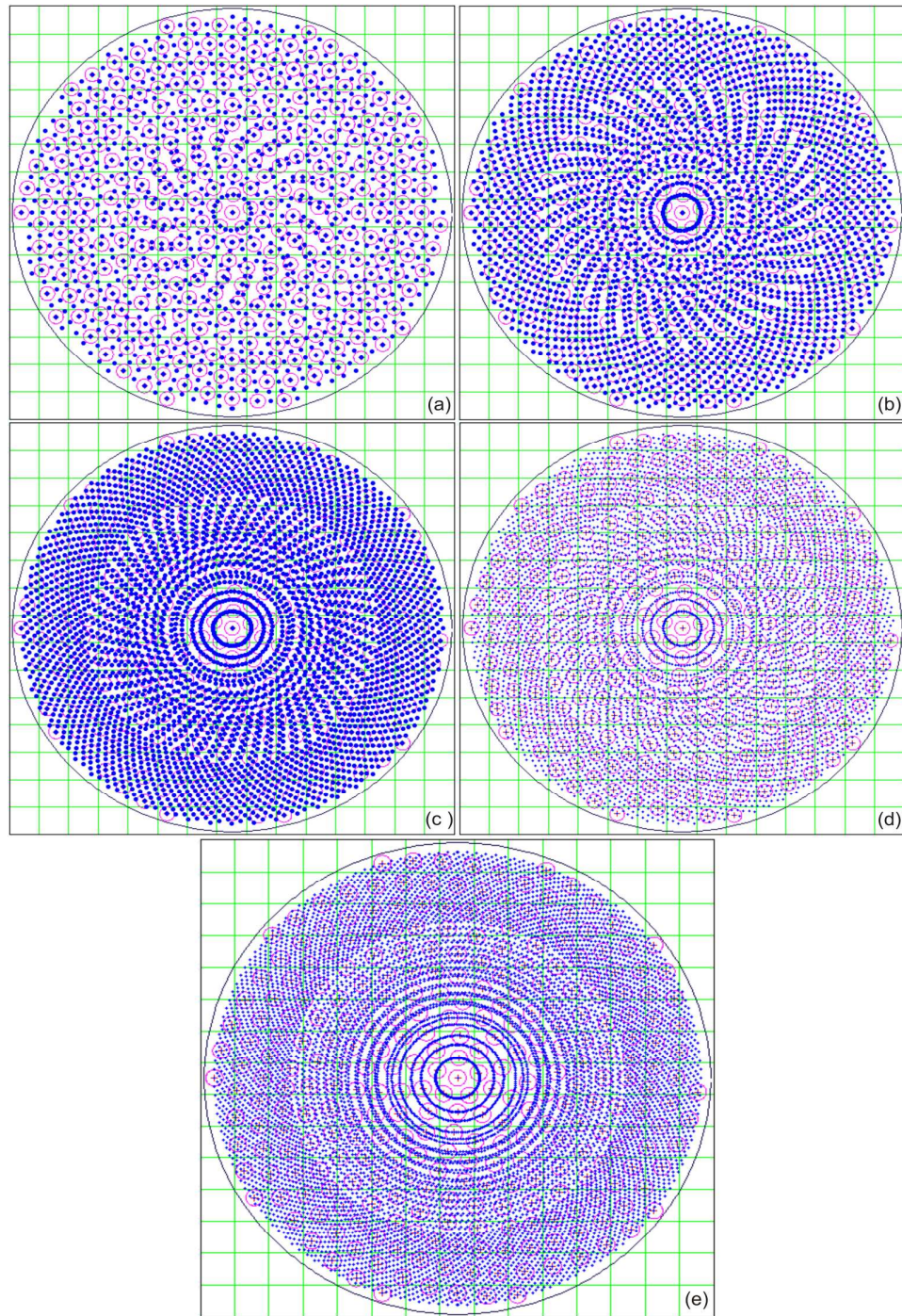
Fig. 5. Sampled points (blue dots) with the screen in Fig. 4 [$n = m = 20$], for different numbers of rotation movements and images: a) $t = 4$, b) $t = 8$, c) $t = 12$, d) $t = 17$, e) $t = 32$; each angular step is $\gamma = 2\pi / t$.

where c is given by Eq. (10), and b-1 is the number of columns between P1 and P2. The direction of the scan is defined by the angle β with the x-axis, so it is given by
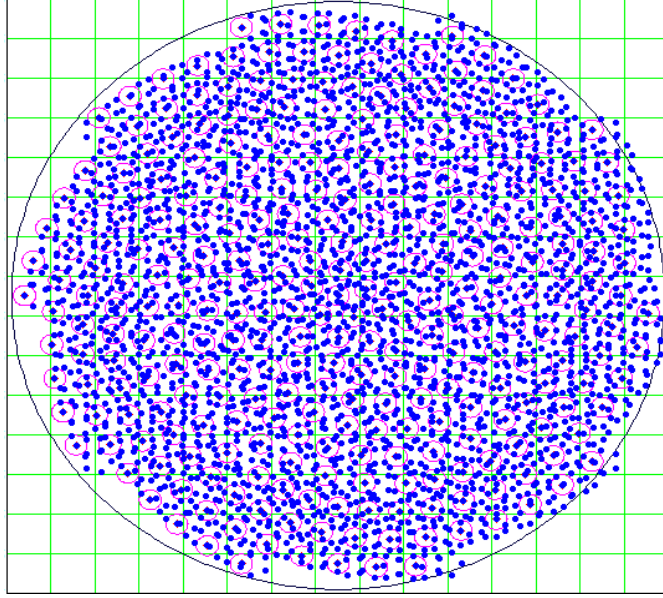
Fig. 6. Sampled points with the screen in Fig. 4 rotated around an axis 3mm to the right of the center of the screen; for this case, $n = m = 20$, $t = 10$, the angular step is $\gamma = 2\pi / t$. The sampling is more uniform even at the center, but the points are distributed more randomly.

$$\beta = \tan^{-1}\left(\frac{1}{b}\right). \tag{13}$$

The distance between P1 and P2 is

$$d = c(1+b^2)^{1/2}. \tag{14}$$

Making s scan steps between points P1 and P2, the size of each step is

$$d_s = \frac{d}{s} = \frac{c(1+b^2)^{1/2}}{s}; \tag{15}$$

this adds s-1 additional points in each square cell. The total number of points for evaluating the surface is

$$T = Ns \approx \frac{1}{4}\pi(m-1)^2 s. \tag{16}$$

3.1 Separation between points

The points on the scan are not equally spaced, with the exception of a few cases (for certain combinations of numbers b and s). In reference to Fig. 7, for any point of the scan (point C), there are six nearby points; these points are on the vertices of a non regular, but symmetric, hexagon (points 2,3, and D, and the other symmetric, three points); so there are three different distances; the distance between points C and D is ds (Eq. (15)), and its x and y projections are given by

$$d_{sx} = d_s \cos\beta = \frac{cb}{s}, \tag{17}$$

and

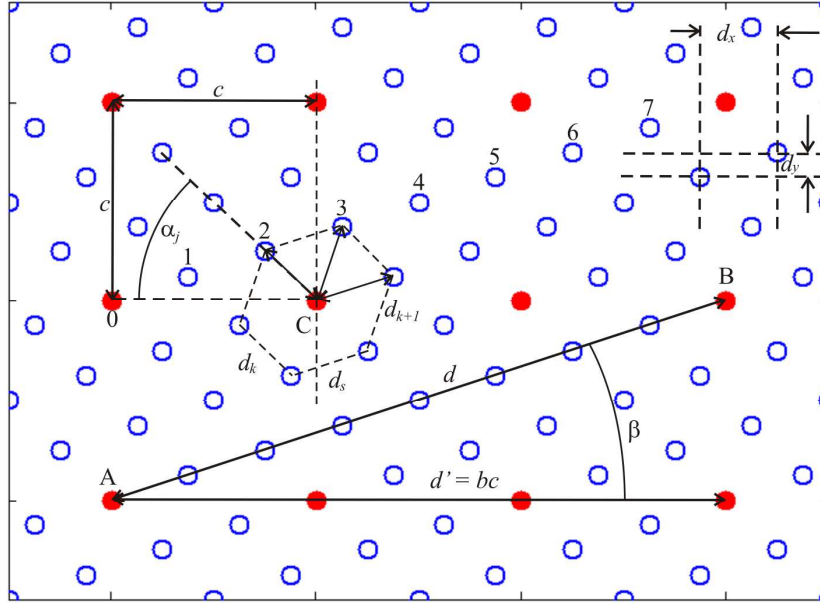$$d_{sy} = d_s \sin \beta = \frac{c}{s}. \tag{18}$$

Fig. 7. Parameters of the scanning of a classical square Hartmann test. Solid dots (red) are the center points for the holes in a classical square Hartmann screen; hollow dots (blue) are the new points added by the scan. In this case: $b = 3$, $s = 8$. Each hole at the classical square Hartmann screen adds *s-1* new evaluation points at the surface; for instance, point 0 gives points 1, 2, 3, …, 7 after the scan. For this example, $k = 2$, $d_2 = 0.354\ c$, $d_3 = 0.395\ c$, $\alpha_2 = 45^0$, $\alpha_3 = -71.565^0$; $d_s = 0.395\ d_{sx} = 0.375$ and $d_{sy} = 0.125$.

For the other distances, it is necessary to find first which two points generated by the scan of point 0 are nearest to the vertical straight line traced from point C (points 2 and 3 in Fig. 7); the number of the left point is given by k as follows

$$k = \text{int}\left(\frac{s}{b}\right) \tag{19}$$

where, the function int(x) gives the integer part of the number x. The number of the point at the right side of the same line is, of course, k + 1. Then, it is not difficult to see that the distance from point C to the j-th point on the line scan from point 0 is

$$d_j = \frac{c}{s}\left[(s - jb)^2 + j^2\right]. \tag{20}$$

Using Eq. (20) for $j = k$ and $j = k + 1$, gives the other two distances; d_s, d_k and d_{k+1}, are the three smaller distances between the scanned points on the surface. The angle α_j is given by

$$\alpha_j = \tan^{-1}\left(\frac{j}{s - jb}\right) \tag{21}$$

To illustrate how the additional points are inserted among the original points, Fig. 8 shows twelve cases with $b = 3$ and $s = 4, 5, 6, \ldots$, and 15; for each case the number of new points added by the scan is s-1, or 3, 4, 5, and 16, respectively. A hexagon is included to show the nearest points around some particular point; the arrow shows the scan direction. In Table 1, geometrical data for the array of evaluation points are listed. These data is useful to know

what are the smallest distances between two points for different number of steps during the scan. Several features of the array of points for different values of s can be drawn from Fig. 8; Table 1, however, quantifies some of them. For instance, Fig. 8.g) seems to be a square array of points, the principal axes of the array being along different directions from the principal axes of the holes on the screen. From Table 1, this assumption can be proved; from the row
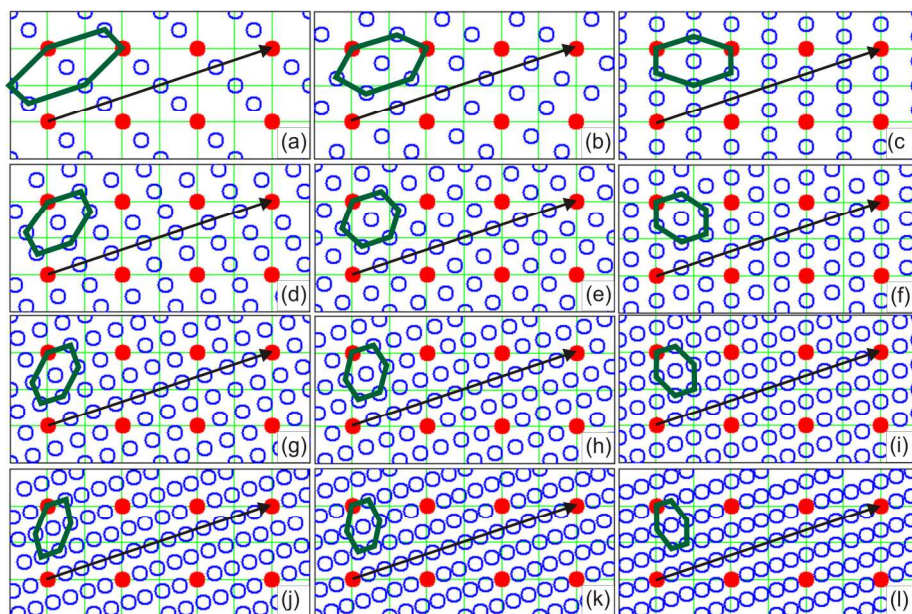

Fig. 8. Examples of additional points added by the scan (hollow blue dots) for the cases a) s = 4, b) s = 5, c) s = 6, d) s = 7, e) s = 8, f) s = 9, g) s = 10, h) s = 11, i) s = 12, j) s = 13, k) s = 14, and l) s = 15. In every case b = 3.

Table 1. Geometrical parameters for the array of evaluation points generated during the linear scan of a classical square Hartmann screen. For these data $b = 3$ and $c = 1$, is used; for all the cases $\beta = 18.435$. Angular data are given in degrees.

s	d_s	d_{sx}	d_{sy}	k	d_{k-1}	d_k	d_{k+1}	α_{k-1}	α_k	α_{k+1}
4	0.7906	0.75	0.25	1	1	0.3536	0.7071	0	45	−45
5	0.6325	0.6	0.2	1	1	0.4472	0.4472	0	26.57	−63.43
6	0.527	0.5	0.1667	2	0.527	0.3333	0.7071	18.43	90	−45
7	0.4518	0.4286	0.1429	2	0.589	0.3194	0.5151	14.04	63.43	−56.31
8	0.3953	0.375	0.125	2	0.6374	0.3536	0.3953	11.31	45	−71.57
9	0.3514	0.3333	0.1111	3	0.4006	0.3333	0.5556	33.69	90	−53.13
10	0.3162	0.3	0.1	3	0.4472	0.3162	0.4472	26.57	71.57	−63.43
11	0.2875	0.2727	0.09091	3	0.4896	0.3278	0.3748	21.8	56.31	−75.96
12	0.2635	0.25	0.08333	4	0.3536	0.3333	0.4859	45	90	−59.04
13	0.2433	0.2308	0.07692	4	0.3846	0.3172	0.4142	36.87	75.96	−68.2
14	0.2259	0.2143	0.07143	4	0.4165	0.3194	0.3642	30.96	63.43	−78.69
15	0.2108	0.2	0.06667	5	0.3333	0.3333	0.4472	53.13	90	−63.43
16	0.1976	0.1875	0.0625	5	0.3536	0.3187	0.3953	45	78.69	−71.57
17	0.186	0.1765	0.05882	5	0.3767	0.3168	0.3578	38.66	68.2	−80.54
18	0.1757	0.1667	0.05556	6	0.3239	0.3333	0.4231	59.04	90	−66.8
19	0.1664	0.1579	0.05263	6	0.337	0.3201	0.3832	51.34	80.54	−74.05
20	0.1581	0.15	0.05	6	0.3536	0.3162	0.3536	45	71.57	−81.87

corresponding to $s = 10$, it is easy to find that $ds = dk$, and $\beta + \alpha_k = 90°$, proving that the array is indeed square. Similar data can be computed for other values of b.

It is worth saying here that in some cases, the $k + 1$-th point is not one of the six nearest points; this point must be replaced by the k-1-th point. This is the case when $k = b/s$, then k is an integer. For this reason, in Table 1, the data for d_{k-1} and α_{k-1} are also included.

4. Experiment

In order to show the feasibility of the proposal and the advantage of including more points during the Hartmann test, the testing of an $F/4$ spherical mirror, with a diameter $D = 150$ mm, and a radius of curvature $r = 600$ mm, was conducted. The number of points along a principal diameter of the mirror was chosen as $m = 11$, according to Eq. (10) the hole separation must be $c = 15$ mm; to avoid part of the holes at the edge being out of the surface the clear diameter was adjusted to 140 mm, so that $c = 14$ mm. According to Eq. (11) the total number of points inside the pupil diameter was around 79, however, due to the adjustment of the diameter the real number was increased to 89. In Fig. 9 the screen design is shown. The starting position of the mirror is defined by the circle; as the screen moves to scan the surface, some holes go out of the pupil, but they are substituted by other holes initially outside the pupil, for that reason the screen is larger than a classical Hartmann screen. According to Fig. 2, a convenient diameter for the holes is 5 mm.
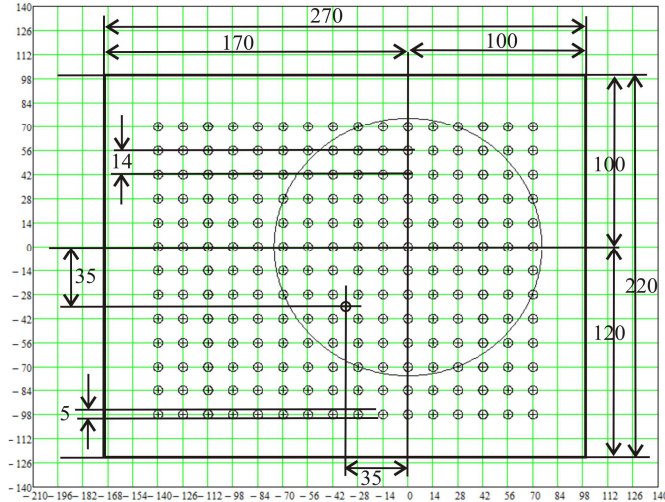
Fig. 9. Design of the Hartmann screen for testing a mirror with scan. The arrow shows the scan direction. Distances are in mm.

In Fig. 10 the experimental setup is shown; the separation between the source and the observing screen is not too small, however, this is not a drawback for the evaluation procedure as will be explained later.

To define the scan path the points P1 and P2 were separated $b = 3$ columns, so the inclination angle β was 18.43° and the number of steps of the scan was chosen to be $s = 9$. The step size was $d_s = 4.92$ mm, the full scan distance $d = 44.28$ mm.

On each step a different picture of the bright spot array was acquired; the total number of evaluated points was 803; i.e., 2 more points than the result of $89 \times s = 801$.

Figure 11 shows the actual screen used for the test and four different pictures of the spots obtained at different positions of the screen during its scan. There is a bright reference spot corresponding to a hole between four adjacent holes to follow the movement of the screen. In Fig. 12 a plot of the 803 centroids is shown.
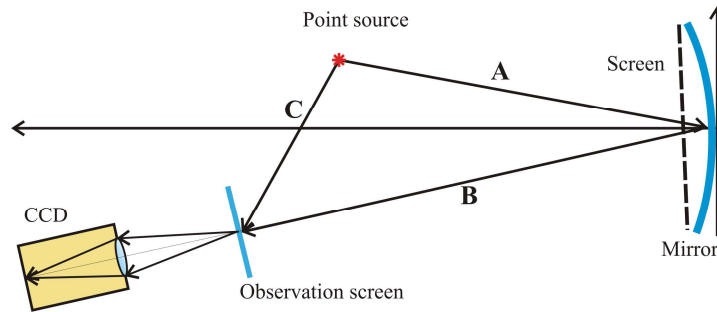

Fig. 10. Experimental setup for the scanning Hartmann test of the spherical mirror. Distances are: A = 585 mm, B = 689 mm, and C = 135 mm
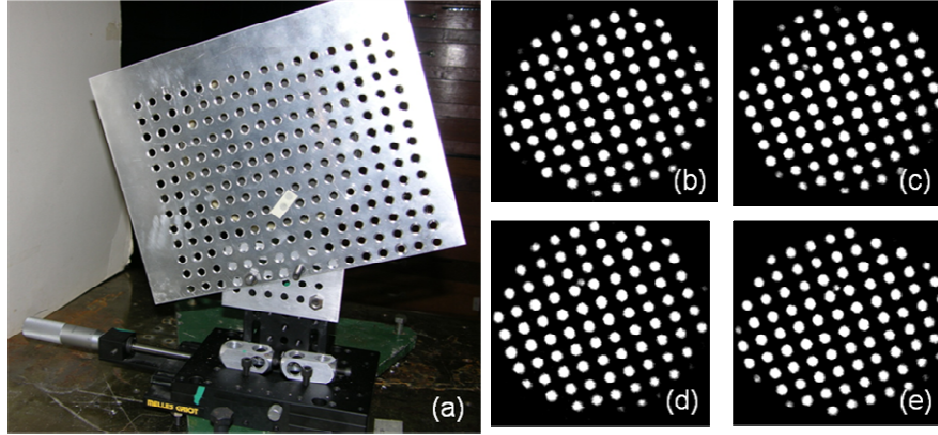
Fig. 11. a) Actual screen for the test; it is inclined and mounted on a precision stage for the scan. The test surface is behind the screen. b) Hartmanngram for the starting position of the screen (0.00 mm); the other images are for c) 9.84 mm, d) 19.68, and e) 29.52 mm.

5. Evaluation of the normals and integration procedure

The normals to the mirror are evaluated according to the following procedure. The real positions of the holes on the screen are measured with the CCD camera, the hole positions on the *xy* plane and the spot positions on the observing screen are well known, then it is an easy task to find the *xyz* components of the incident and reflected rays on the mirror for each hole of the screen. In reference to Fig. 13, as the magnitudes of vectors $\mathbf{V}_1$, $\mathbf{V}_2$, and $\mathbf{V}_3$ are known from the setup (Fig. 10), their directions are easily found. Then the incident ray can be expressed as

$$\mathbf{R}_i = \mathbf{V}_1 + \mathbf{H}, \tag{22}$$

and the reflected ray is found by

$$\mathbf{R}_r = \mathbf{V}_2 + \mathbf{S} - \mathbf{H}, \tag{23}$$

where $\mathbf{H}$ and $\mathbf{S}$ are, respectively, the vector for a hole on the screen and for its corresponding spot at the observing screen. According to the Reflection Law, the normal to the surface at the point of incidence is

$$\mathbf{N} = \frac{\mathbf{r}_r - \mathbf{r}_i}{\|\mathbf{r}_r - \mathbf{r}_i\|}, \tag{24}$$

where $\mathbf{r}_i$ and $\mathbf{r}_r$ are the unit vectors associated with the incident and reflected rays. Once the normals to the test surface are obtained, the shape of the surface can be found by using the integral

$$z - z_o = -\int \left(\frac{n_x}{n_z} dx + \frac{n_y}{n_z} dy \right); \tag{25}$$

Equation (20) was initially proposed by R. Díaz-Uribe [5], and has been successfully used by him and his associates [3], [5], [6]
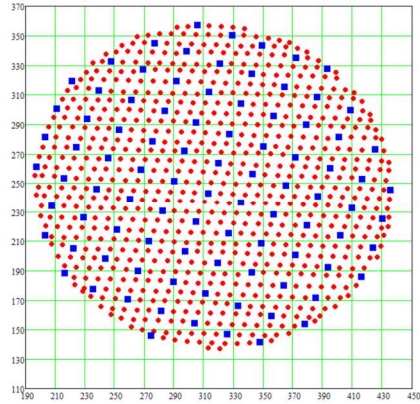
Fig. 12. Evaluated positions of the centroids of the 9 images (in pixels); the blue squares are the centroids obtained for image in Fig. 11.b) at the starting position of the screen. For each position ten images are averaged to reduce the noise.

The integral in Eq. (20) is a path integral that can be computed with the trapezoid rule along different polygonal paths, going over the positions of the holes of the screen during the scan, in every vertex of the polygonal path there is a hole position. The integral in Eq. (20) can be found with exception of an arbitrary integration constant z_o. Then, in order to have only one constant, all the integration paths must start at the same point and to reduce the numerical calculation error the paths must be as simple and direct as possible; very involved paths increase the numerical error.
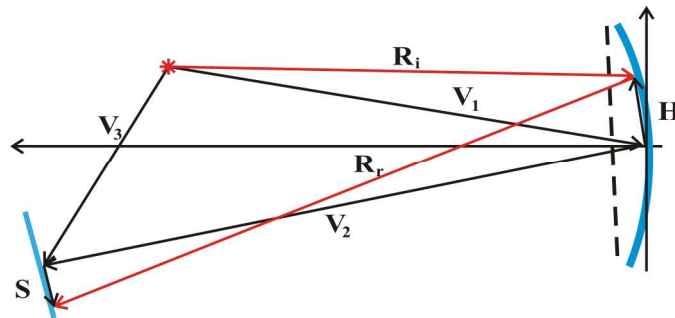

Fig. 13. Diagram to explain the vectors involved in the calculation of the normal of the test surface.

In order to compare the proposed method with the classical Hartmann test without scan, two evaluations were performed: the first was made with only the first image (89 evaluation points), while for the second all the 803 points obtained with the scan were used. In Fig. 14 the integration paths for both cases are shown. After performing the integration procedure, and fitting the best surface to the result, the differences are shown in Fig. 15. Essentially both Figs. 15 a) and b), show the same results; it is clear, however, that Fig. 15.b) shows more details of the surface, the lateral resolution of the test has been improved.
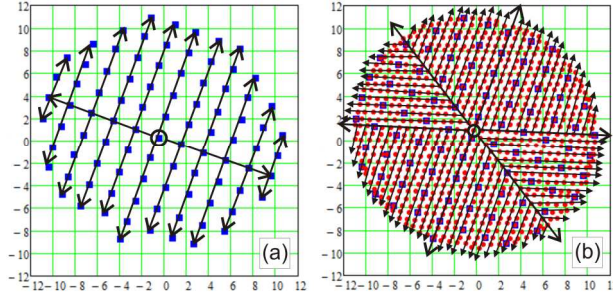
Fig. 14. Integration paths for evaluating the surface with a) only one image (89 points), and b) with the 9 images (803 points). Distances are in mm.
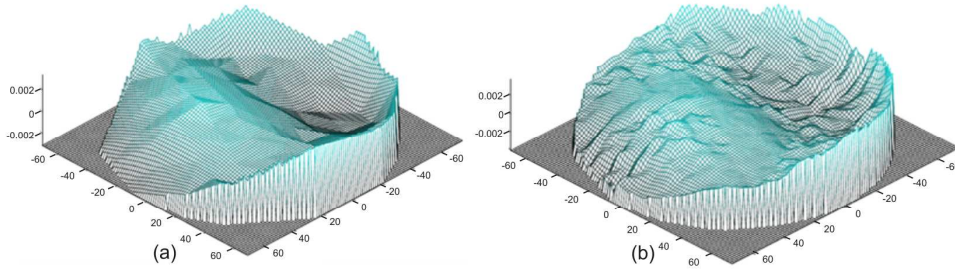

Fig. 15. Surface differences from the best fit surface. A) Results obtained with 90 points from only one image b) Results obtained for all the 803 points obtained from the 9 images of the scan. All distances are in mm.

Unfortunately, this experiment has not been able to show that the truncation errors can also be reduced. There is a simple explanation for this result: the truncation error due to the trapezoid rule is bounded by [3]

$$|\varepsilon| \le \frac{h^2}{12}(b-a)M, \qquad (26)$$

where h is the average separation between adjacent points along the integration path, $b - a$ is the total length of the integration path, and $M = [d^2f(x)/dx^2]_{max}$, is the maximum value of the second derivative of the integrating function $f(x)$. Then, as a sphere is a second degree surface, it can be expressed in the zx –plane as

$$z(x) = Ax^2 + Bx + C, \qquad (27)$$

where A, B and C are arbitrary constants $(A \ne 0)$. The normal to this curve is obtained through the derivative of Eq. (22),

$$\mathbf{N}(x, z) = \left(2Ax + B\right)\hat{i} - \hat{k}, \qquad (28)$$

then, according to Eq. (20) the integrating function is

$$f(x) = \frac{N_x}{N_z} = -2Ax - B. \qquad (29)$$

It is clear that the second derivative of $f(x)$ in Eq. (24) is null and so is M in Eq. (21); in consequence, the truncation error in Eq. (21) is negligible not only for spheres, but also for all the conic surfaces, when the trapezoid rule is used. The error is not zero because, this is true only for ideal conics. Important truncation errors are introduced for very fast surfaces where the fabrication errors make the surface depart appreciably from the ideal surface.

6. Conclusions

In this paper the scanning of a classical Hartmann screen has been proposed; after each step of the scan a different image of the bright spots is obtained. This allows the introduction of many more evaluation points than for the classical static case. Basic ideas about how to design radial and square screens have been presented. For radial screens a spiral arrangement of the holes is useful to introduce new evaluation points along the radial and azimuthal directions. The main advantage of this kind of screens is that the scan is performed by only a rotation of the screen; the main drawback is that the evaluation points are more crowded at the center of the pupil whereas at its rim they are much more separated. In an attempt to overcome this problem, a different design was proposed: first of all, a spiral screen with a very high density of points was designed; then, only those points having a minimum distance with some others are included in the final design.

For square screens, a classical design was used, the key to introduce more evaluation points along the x and y directions, is to linearly scan the screen along a direction different from the main directions defined by the square array of holes. Some equations have been deduced, which account for some geometrical features of the full array of evaluation points.

The feasibility of this proposal has been shown by scanning a square screen during the test of a spherical surface. In the testing of such a surface, a comparison was made for the evaluation of the surface with only one image and with nine images obtained along the scan; it has been shown that more information is obtained by scanning the screen, improving the lateral resolution of the test. In this case, however, the size of screen must be larger than for the static method.

Acknowledgments